On Analysis of Chemical Reactions Coupled Gas Flows in SOFCs

Jinliang YUAN[1,*], Guogang YANG[2], Bengt SUNDÉN[1]

* Corresponding author: Tel.: ++46 (0)46 222 4813; Fax: ++46 (0) 46 222 4717; Email: jinliang.yuan@energy.lth.se
1: Department of Energy Sciences, Faculty of Engineering,
Lund University, Box 118, 22100 Lund, Sweden
2: Marine Engineering College, Dalian Maritime University, Dalian 116026, China

Abstract Solid oxide fuel cell (SOFC) is among others one of the most promising technologies for electricity energy generation. A recent new trends is to reduce its operating temperature from 1000^{o}C to 800^{o}C by employing a thick porous layer as the supporting structure. Various transport processes occurred are strongly affected by catalytic chemical/electrochemical reactions appearing in nano- or/and microstructured and multi-functional porous electrodes. It is particularly true if methane is used as the fuel, and internal reforming reactions within the microstructured porous anodes enable the conversion of the methane into H_2 and CO. To deeply understand the chemical reaction coupled gas flow and heat transfer in the microstructured porous anode, a fully three-dimensional numerical calculation procedure (CFD) is developed and applied. The species mass/heat generation and consumption related to the internal reforming reactions and the electrochemical reaction have been identified and employed in the study. The variable thermal-physical properties and transport parameters of the fuel gas mixture have also been taken into account. Furthermore, the heat transfer due to the fuel gas flow is implemented into the energy balance based on multi-component diffusion models. Finally, various issues connecting to the micro models of the surface reactions are discussed and reviewed.

Keywords: Gas Flow, Chemical Reactions, Micro Porous Materials, SOFC

1. Introduction

Solid oxide fuel cell is one of the most promising technologies for electricity energy generation, because of its high energy conversion efficiency, environmental friend-liness and flexibility of usable fuel types. Many variations of SOFC designs are possible, like tubular, planar and monolithic. The planar SOFCs have several advantages, such as higher power density, compactness, and simple to be fabricated and manufactured into various configurations [1-3].

One of the new trends is to reduce the operating temperature of SOFCs to an intermediate range (from 1000 ^{o}C to 800 ^{o}C) by employing a thick porous layer (1.5-2 mm) as the supporting structure. There are various transport processes strongly affected by catalytic chemical/electrochemical reactions in nano- or/and microstructured and multi-functional porous electrodes. The transport rate of fuel gases in the microstructured porous anode is controlled by various parameters, such as porous microstructure (i.e., pore size, permeability, volume percent porosity of the employed microstructured porous layer), pressure gradient between the fuel flow duct and the microstructured porous anode, gas composition and inlet conditions, etc [1-7].

For the case of pure hydrogen being employed as a fuel, part of H_2 is consumed while water vapor (H_2O) is generated during the electrochemical reaction in the active regions between the microstructured porous anode and the electrolyte. If methane is used as the fuel, internal reforming reactions within the microstructured porous anodes enable the conversion of the methane into H_2 and CO. In this case, several benefits are expected to have internal steam reforming of hydrocarbon fuels, e.g., the energy conversion efficiency will be

much higher. Moreover, close coupling of the internal reforming and the electrochemical reactions at the microstructured porous anode gives good heat transfer. Furthermore, H_2 and CO are utilized by the cells as soon as they are produced by the reforming reaction, and the steam produced by the electrochemical reaction can be used in the reforming reaction as well [8,9].

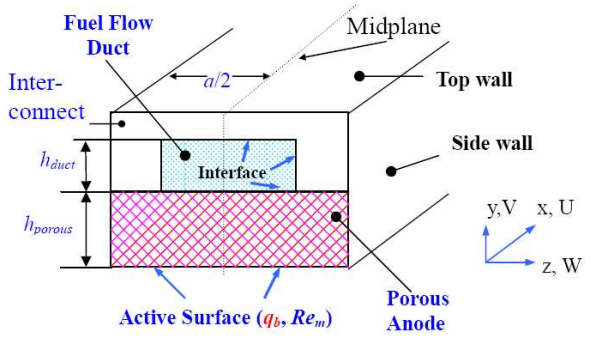

Fig. 1. A schematic drawing of the anode.

To deeply understand the chemical reaction coupled gas flow and heat transfer in the microstructured porous anode, a fully three-dimensional numerical calculation procedure (CFD) is developed and applied. The study includes the steam internal reforming reaction of CH_4 and the shift reactions of CO. The investigated duct includes the microstructured porous anode, fuel gas flow duct and the solid interconnects, as shown in Fig. 1. By calculating catalytic reaction rates, the surface reaction effects on the species mass/heat generation and consumption have been identified and implemented in the study. The variable thermal-physical properties and transport parameters of the fuel gas mixture have also been taken into account. Furthermore, the heat transfer due to the fuel gas flow is implemented into the energy balance based on multi-component diffusion models. One of the objectives of this study is to develop such an approach to understand the gas flow and heat transfer coupled by the chemical reactions in the composite domains including the microstructured porous anode in the intermediate temperature SOFCs.

2. Problem Statement and Modelling

As shown in Fig. 1, the U, V, and W are the velocity components in the x, y and z directions, respectively. In this paper, a fully three-dimensional computational fluid dynamics (CFD) approach is developed to numerically simulate and analyse the chemical reactions and coupled heat transfer.

In this study, the microstructured porous anode is assumed to be homogeneous and characterized by effective parameters and the fuel species in the microstructured porous anode are in thermal equilibrium with the solid matrix. The electrochemical reactions to generate electricity are the oxidation of H_2:

$$H_2 + O^{2-} \rightarrow H_2O + 2e^-$$
$$\Delta H_{(1000\ \mathrm{K})} = -248\ \mathrm{kJ/mol} \qquad (1)$$

The above reactions produce a significant amount of water and heat at the anode/ electrolyte interface during operation. Methane and carbon monoxide can be internally reformed into H_2 by the following reactions:

$$CH_4 + H_2O \rightarrow CO + 3H_2$$
$$\Delta H_{(1000\ \mathrm{K})} = 226\ \mathrm{kJ/mol} \qquad (2)$$
$$CO + H_2O \rightarrow CO_2 + H_2$$
$$\Delta H_{(1000\ \mathrm{K})} = -35\ \mathrm{kJ/mol} \qquad (3)$$

Equation (2) is internal steam reforming reaction, while Eq. (3) is usually referred to as water-gas shift reaction. It should be mentioned that the steam reforming reaction is endothermic and the overall balance of the reaction requires net heat input by the electrochemical reactions.

The governing equations to be solved are the continuity, momentum, energy and species equations. The inclusion of the source term allows the moment equation to be valid for both the microstructured porous anode and the fuel gas flow duct. For the microstructured porous anode, the source term is not zero, and the momentum equation with the non-zero source term can be regarded as a generalized Darcy model.

The species conservation equations are also formulated in a general form, and solved for H_2, CH_4, CO and H_2O, respectively. The Stefan-Maxwell model is applied for multi-

component system as in this study. The diffusion coefficients of species *i* in the fuel gas flow duct are calculated by the expression based on the binary coefficients. The governing equations are coupled by the current density, temperature, fuel species partial pressure/concentration via source terms and variable physical/transport properties. It is clear that no gas flow is present in the solid interconnect. The continuity, momentum and species equations are then blocked out and only the heat conduction equation is solved for this domain [9].

Table 1. Governing equations and relevant non-zero sources terms.

	Governing equations	Non-zero sources terms	Sub-domain
Continuity equation	$\nabla \bullet (\rho_{\text{eff}} \mathbf{v}) = S_m$	$S_m = (J_{\text{H}_2} + J_{\text{H}_2\text{O}}) \frac{A_{\text{active}}}{V}$ $= (-\frac{i_{H_2}}{2F} M_{\text{H}_2} + \frac{i_{\text{H}_2}}{2F} M_{\text{H}_2\text{O}}) \frac{A_{\text{active}}}{V}$	Bottom wall
Momentum equation	$\nabla \bullet (\rho_{\text{eff}} \mathbf{vv}) = -\nabla P + \nabla \bullet (\mu_{\text{eff}} \nabla \mathbf{v}) + S_{\text{di}}$	$S_{\text{di}} = -(\mu_{\text{eff}} \mathbf{V} / \beta)$	Porous anode
Species equation	$\nabla \bullet (\rho_{\text{eff}} \mathbf{V} Y_i) = \nabla \dot{\mathbf{m}}_i + S_{s,i}$	$S_{s,\text{H}_2} = (3R_r + R_s) M_{\text{H}_2}; S_{s,\text{CH}_4} = -R_r M_{\text{CH}_4};$ $S_{s,\text{H}_2\text{O}} = (-R_r - R_s) M_{\text{H}_2\text{O}}; S_{s,\text{CO}} = (R_r - R_s) M_{\text{CO}}$	Porous anode
Energy equation	$\rho_{\text{eff}} c_{p,\text{eff}} \nabla \bullet (\mathbf{v}T) = \nabla \bullet (k_{\text{eff}} \nabla T$ $- \sum_{i=1}^{n} \dot{\mathbf{m}}_i h_i) + S_T$	$S_T = \sum_i R_i \Delta h_{\text{reaction},i}$	Porous anode

It should be noted that, in order to include the Knudsen diffusion flux, the coefficient $D_{i,k}$ is calculated based on the free molecular flow theory [13]:

$$D_{i,k} = \frac{2}{3} r_e v_i = \frac{2}{3} r_e \sqrt{\frac{8\Re T}{\pi M_i}} \tag{5}$$

in which r_e is the effective radius and v_i the average molecular speed of the *i*th fuel species. By accounting for the reduction in the cross-sectional area due to the solid matrix (evaluated by the porosity) and the increased diffusion length due to the tortuous paths of real pores in the porous anode (evaluated by the tortuosity), the effective diffusion coefficient is evaluated [12, 13]:

$$D_{i,\text{eff}} = \frac{\varepsilon}{\tau} (\frac{D_{i,gm} \times D_{i,k}}{D_{i,gm} + D_{i,k}}) \tag{6}$$

where ε is the porous anode porosity, τ tortuosity. $D_{i,gm}$ is the *i*th species molecular diffusion coefficient in the fuel gas mixture.

In this study, it is assumed that the anode material is nickel/zirconia cermet which can provide sufficient activity for the steam reforming and the water-gas shift reactions [14]. As for the kinetics of the methane reforming reaction on the concerned catalysts, it is common to employ the overall forward kinetic reforming reactions, and the first order kinetic expression is generally applied for the direct internal reforming reactions in SOFC [10, 11]. The following relations are employed to express the kinetic rates of absorption or production of the fuel gas species, based on local partial pressure, temperature and species compositions:

$$R_r = k_r^+ p_{\text{CH}_4} p_{\text{H}_2\text{O}} - k_r^- p_{\text{CO}} (p_{\text{H}_2})^3 \tag{7}$$

$$R_s = k_s^+ p_{\text{CO}} p_{\text{H}_2\text{O}} - k_s^- p_{\text{CO}_2} p_{\text{H}_2} \tag{8}$$

in which, k^+ and k^- are velocity constants of the forward and backward reactions, *p* partial pressure.

$$k^+ = k_0 F(p_i) exp(-\frac{E_a}{\Re T}) \tag{9}$$

where $\Re$ is the universal gas constant with unit J/(mol K), *F* the function of the species partial pressure, while E_a stands for the activation energy, k_0 the pre-exponential constant. The first order kinetic expression is applied for the direct internal reforming reactions in SOFC [9-11].

$$k_r^+ = 2395 exp(-231266/\Re T) \tag{10}$$

$$k_s^+ = 0.0171 exp(-103191/\Re T) \tag{11}$$

The backward kinetics k_r^- and k_s^- can be determined based on the following equilibrium constants K_e for the two reactions,

$$K_{er} = \frac{k_r^+}{k_r^-}; K_{es} = \frac{k_s^+}{k_s^-} \quad (12)$$

which are functions of temperature given by the following empirical equations [11]:

$$K_{er} = 1.0267 \times 10^{10} \times exp(-0.2513Z^4 + 0.3665Z^3 + 0.5810Z^2 - 27.134Z + 3.27770) \quad (13)$$

$$K_{es} = exp(-0.2935Z^3 + 0.6351Z^2 + 4.1788Z + 0.3169) \quad (14)$$

$$Z = \frac{1000}{T} - 1 \quad (15)$$

It should be noted that fuel gas mass fraction/flux boundary conditions are specified at the external walls in this study. For the temperature boundary conditions, the thermal insulation is put on the walls (the top and side ones), and a constant heat flux condition is specified at the active surface, as discussed in [11]. It is worth to point out that the thermal conditions at the top and side interfaces are implicitly obtained by thermal coupling through the top/side interfaces, while all the conditions at the bottom interface (between the fuel flow duct and the porous anode in Fig. 1) by coupling the mass, heat and species transfer. As revealed in this study, the obtained thermal conditions at the interfaces are characterized by axially varying interface heat fluxes (or temperature gradients) and interface temperatures. As expected, this is due to the complex hydrodynamic and thermal transport interactions by the chemical reactions, species flux through the porous reaction layer, and the convective flows in the gas flow duct.

By the convective mass, flow, and temperature distributions calculated by the governing equations above, the thermal performance at the interfaces can be evaluated by the average interface temperature and its gradient, or by the dimensionless Nusselt number:

$$\overline{Nu}_i = \frac{\bar{h}_i D_h}{k_{eff}} = \frac{(dT/dx)_i D_h}{(\bar{T}_i - T_{bulk})} \quad (16)$$

$\bar{T}_i$ is the spanwise average temperature at the interface i, $(dT/dx)_i$ the interface temperature gradient, T_{bulk} the mean (bulk) streamwise gas flow temperature in the cross-section,

$$T_{bulk} = \frac{\int T|U|dA}{\int |U|dA} \quad (17)$$

It is worthwhile to note that the approach applied in this study is based on one set of governing equations with extra source terms and the local transport properties' implementation, to treat the porous layer and pure gas flow regions as a single domain. The code is generally based on the finite-volume technique with boundary fitted coordinates for solving the differential equations [11]. As shown above, the equations needed for the calculation are coupled by the temperature, fuel species partial pressure/concentration via source terms and variable physical/transport properties. The source term in the continuity equation is zero in most of the regions, and non-zero only in the regions neighboring boundaries, where mass transfer caused by the electrochemical reaction occurs (the bottom wall in Fig. 1). It is a fact that no gas flow is present in the solid interconnect. The continuity, momentum and species equations are then blocked out and only the heat conduction equation, derived from the energy equation, is solved for this domain. As mentioned earlier, the thermal physical/transport properties of the fuel gas mixture are variable. All the parameters are calculated and updated during iterations of the calculation.

3. Results and Discussion

Common cell configuration parameters are applied: length of the duct L = 20 mm; width of the porous layer a = 2 mm, and its thickness h_p = 2 mm; while the width of the flow duct is b = 1 mm, and its height h_d = 1 mm. Fuel gas inlet conditions are: temperature T_{in} = 800 ^oC, partially (30%) prereformed methane/steam mixture with: Re_{in} = 50, molar concentration X_{H2}:X_{CH4}:X_{CO}:X_{H2O}:X_{CO2}=0.280:0.171:0.023: 0.473:0.053; In the porous layer, typical values are employed for porosity ε =0.5, tortuosity τ =3, and permeability β = 2×10^{-10} m^2; In this study, a constant current density i = 0.6 A/cm^2 is prescribed.

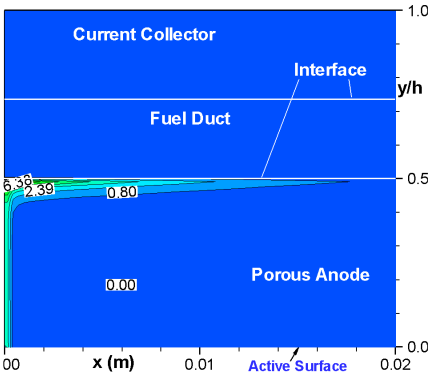

Fig. 2. Distribution of steam reforming reaction rate R_r.

The calculated steam reforming reaction rate is shown in Fig. 2. It is found that the reaction is strong at the interface and the entrance regions within the porous anode close to the fuel flow duct and no reactions can be observed in the rest of the porous anode, particularly after a certain distance downstream the inlet. This is so because there is strong fuel gas permeation to the porous anode due to large pressure gradients, and the methane is completely reformed (not shown here). It should be mentioned that a similar trend is found for the water-gas shift reaction rate distribution.

A noteworthy feature of the conjugated calculation and analysis in this work is the characterization of the thermal boundary condition development close to the interfaces between the fuel gas flow duct and the solid plates/the porous layer. This is achieved by the coupling of the mass, momentum, heat and fuel gas species with the chemical reactions. As shown in Fig. 3, the average temperature distributions at the top, side and bottom interfaces (Fig. 1) are axially varying along the main flow direction. It is found that the bottom interface temperature is higher than the fuel gas inlet temperature and cell operating temperature (800°C at the base condition). Furthermore, the temperature gradient at the bottom interface displays a trend, i.e., increasing sharply from the duct entrance, and maintaining almost a constant value until the duct exit as shown in Fig. 4. The curves essentially describe the convective thermal boundary layer development in the gas flow duct.

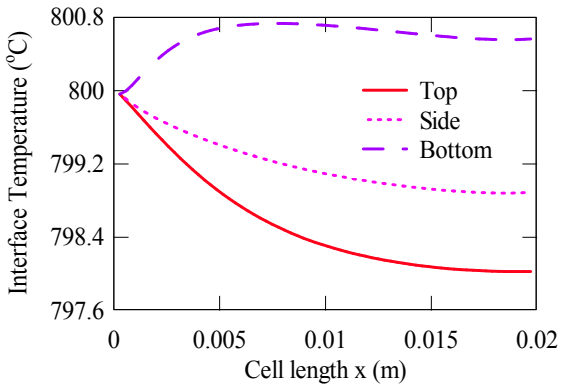

Fig. 3. Interface temperature profiles along the main flow direction at base condition.

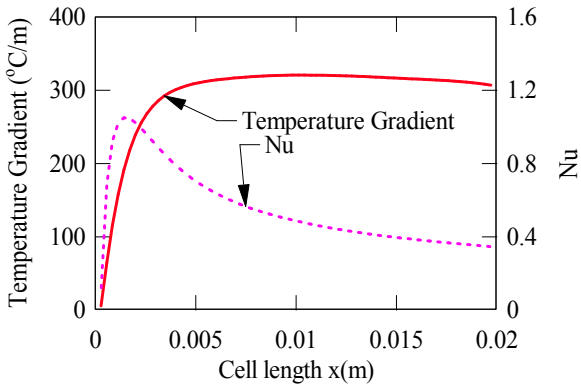

Fig. 4. Bottom interface temperature gradient and Nusselt number profiles along the main flow direction at base condition.

The consequent impact of the altered interface temperature and its gradient on the convective heat transfer coefficient is plotted in Fig. 4 as well. It is obvious that the classical duct thermal boundary conditions (constant heat flux or wall temperature or the combined ones on the walls) are not rigorously applicable for the chemical reaction coupled heat transfer, in which the heat source/sink in the porous anode and the heat conduction in the solid plates are involved. As revealed, the real thermal interface represents axial variations in both the wall heat flux and the surface temperature due to the involved chemical reactions, which requires a conjugated treatment of the mass transfer, gas flow, heat transport and chemical reactions in various functional components. Due to the big mass permeation into the porous anode and large reforming reaction rate close to the inlet

region, Nu increases in the entrance region along the main flow direction and reaches a maximum value. It decreases steadily afterwards, as shown in Fig. 4, because both the mass permeation and the reforming reaction become weaker.

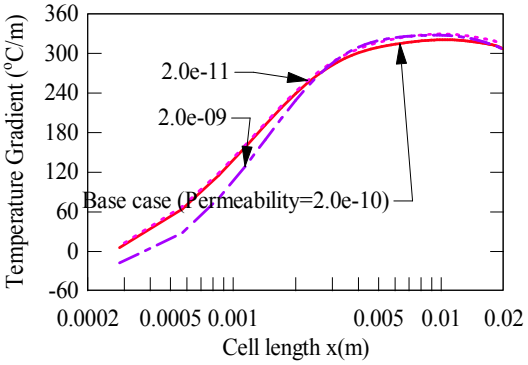

a)

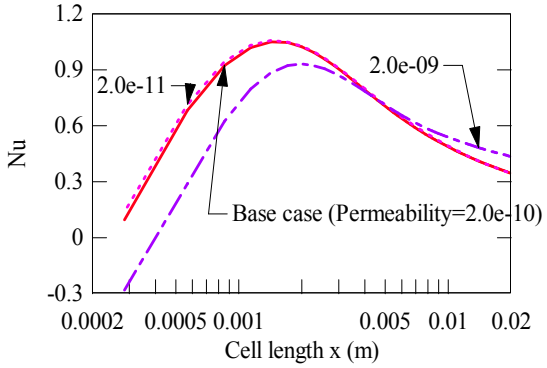

b)

Fig. 5. Permeability effects on: a) temperature gradient; and b) Nusselt number at the bottom interface.

Figure 5 shows the effects of the porous layer permeability on the convective heat transfer at the bottom interface. By the simulated results, it is found that the thermal boundary development at the bottom interface is prominent, in terms of variation of the interface temperature and its gradient (not shown in this study). This trend is enhanced if the big permeability (β=2×10^{-9} m^2) is employed, as shown in Fig. 5. For the porous anode with a small permeability (β=2×10^{-11}m^2), almost the same temperature gradient and Nu as for the base case are identified in Fig. 5.

Figure 6 shows the steam reforming reaction rate profiles for various operating temperatures. It is found that the reforming reaction appears in a big region in both the main flow stream and the vertical direction at a lower temperature, i.e., 700°C in Fig. 6*a*, compared to 900 °C in Fig. 6*b*. This is so because the internal steam reforming reactions depend on the local temperature, i.e., higher operating temperature promotes faster reactions. Consequently, bigger values of the maximum reaction rates are expected for the case with high operating temperature.

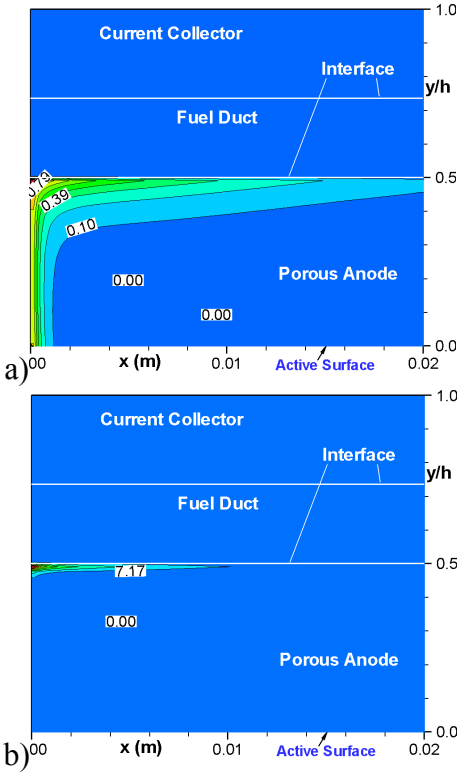

Fig. 6. Steam reforming reaction rate R_r at: a) 700°C; and b) 900 °C.

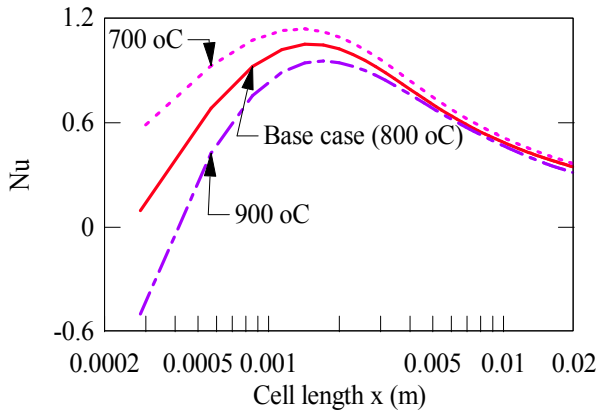

Fig. 7. Operating temperature effect on Nusselt number distribution at the bottom interface along the main flow direction.

From Figure 6a, it is found that the steam reforming reaction happens in a thick area but with weak reforming reactions within the porous anode for a low temperature (700^{o}C). On the other hand, the reforming reaction limits within a thinner region, but a big reaction rate is reached for the case of high temperature (900^{o}C). Compared to the base case, the heat consumption required by the steam reforming reaction varies, which in turn induces strong effects on the convective heat transfer coefficient or Nu within the entrance region, as shown in Fig. 7.

It is clear that the thermal conditions (the average temperature gradient and temperature distributions) and the convective heat transfer coefficient at the bottom interface are axially varying and stronger than those for the top and side interfaces. This finding is true particularly for a case with big porous anode permeability or high operating temperature. It may be due to the fact that the bottom interface involves the more complex mass flow and heat transfer by the conjugated porous material and the reforming reactions. It could suggest that more attention is needed for this interface involving the coupled transport processes and chemical reactions if SOFC optimizating design is prevailing.

4. Multiscale Models

It is a fact that truly functional and predictive capabilities of SOFC models remain a challenge due to inadequate macroscopic modeling and resolution of active interface zone between the electrode and electrolyte, and existence of a wide range of characteristic length and time scales. For instance, gas-phase flow and heat transfer in the reactants flow duct are in mm-cm scale, while the gas-phase and charge transport within the porous electrodes in μm-mm scale. However the surface transport towards the three-phase boundaries (TPB) and surface reactions are in nm-μm scale [15].

There are several methods suitable for particular length and time scales to treat, for example, aspects of materials phenomena that operate over those scales. In general, the microscale models, such as Density Functional Theory (DFT) and Molecular Dynamics (MD) correspond to the atom or molecular level when thermo- or fluid dynamics is studied. The mesoscale models like Monte Carlo (MC) methods correspond to a larger scale than a particle but a smaller than the facility or the global flow field. The macroscale models, such as CFD in this study, are mainly based on the continuum equations and match to the global flow field. The microscopic models should be able to account for multi-species diffusion and/or convection, and the elementary electrochemical reaction kinetics, proton or ion transport in the micro-structured porous electrodes and electrolytes. The following issues may be also addressed in the micro models, i.e., where exactly are the reactions occurring in the nano-/micro-scaled porous structures; what are the reaction rate determining steps; whether the rate determining steps depend on the operating temperature and other parameters?

Two multiscale modelling approaches originated from material sciences for different time- and length scales are possible for catalytic chemical reaction coupled gas flow problems as appeared in fuel cells. For the first approach, the modeling starts at higher resolution (smaller scale) and properties are extracted and used as input to the next level method. This one is to date the most developed method for multiscale modeling. For the latter one, there are different ways to describe the concerned regions with the appropriate time and length scale resolutions. In this case, only one calculation needs to be preformed, however it requires more computational power compared to the first method [16].

5. Conclusions

In this study, a CFD approach is presented to analyze chemical reactions coupled with heat transfer in a channel relevant for SOFCs. Momentum and heat transport together with gas species equations are solved by coupled source terms, variable thermo-physical and transport properties of the fuel gas species. The effects of the porous layer permeability and the

cell operating temperature on the chemical reactions and convective heat transfer are discussed as well. It is found that either the average temperature gradients (heat flux) or the interface temperatures at the top-, side- and bottom interfaces are axially varying along the main flow direction. The big permeability of the porous layer and high operating temperature promote this variation when the other design and operating parameters are kept constant.

Acknowledgement

The Swedish Research Council (VR) and the National Natural Science Foundation of China (NSFC-50706004) support the current research.

References

[1] Klein, J.M., Bultel, Y., Pons, M. and Ozil, P., 2007, Modeling of a Solid Oxide Fuel Cell Fueled by Methane: Analysis of Carbon Deposition, *J. Fuel Cell Sci. Tech*., 4, 425-434.

[2] Magar, Y.N. and Manglik, R.M., 2007, Modeling of Convective Heat and Mass Transfer Characteristics of Anode-Supported Planar Solid Oxide Fuel Cells, *J. Fuel Cell Sci. Tech*., 4, 185-193.

[3] Daun, K.J., Beale, S.B., Liu, F. and Smallwood, G.J., 2006, Radiation Heat Transfer in Planar SOFC electrolytes, *J. Power Sources,* 157, 302-310.

[4] Hussain, M.M., Li, X., and Dincer, I., 2006, Mathematical Modeling of Planar Solid Oxide Fuel Cells. *J. Power Sources,* 161, 1012-1022.

[5] Virkar, A.V., Chen, J., Tanner, C.W. and Kim, J.W., 2000, The Role of Electrode Microstructure on Activation and Concentration Polarizations in Solid Oxide Fuel Cells. *Solid State Ionics,* 131, 189-198.

[6] Yakabe, H., Hishinuma, M., Uratani, M., Matsuzaki, Y. and Yasuda, I., 2000, Evaluation and Modeling of Performance of Anode-supported Solid Oxide Fuel Cell. *J. Power Sources,* 86, 423-431.

[7] Lehnert, W., Meusinger, J. and Thom, F., 2000, Modelling of Gas Transport Phenomena in SOFC Anodes. *J. Power Sources,* 87, 57-63.

[8] Ackmann, T., Haart, L.G.J., Lehnert, W. and Thom, F., Modelling of Mass and Heat Transport in Thick-Substrate Thin-Electrolyte Layer SOFCs. *Proc. 4th European Solid Oxide Fuel Cell Forum 2000*, Lucerne/Switzerland, 431-438.

[9] Yuan, J., Rokni, M. and Sundén, B., 2003, Three-Dimensional Computational Analysis of Gas and Heat Transport Phenomena in Ducts Relevant for Anode-Supported Solid Oxide Fuel Cells. *Int. J. Heat Mass Transfer,* 46, 809-821.

[10] Barzi, Y.M., Ghassemi, M., Hamedi, M.H. and Afshari, E., 2007, Numerical Analysis of Output Characteristics of a Tubular SOFC with Different Fuel Compositions and Mass Flow Rates. In: Proceedings of *Solid Oxide Fuel Cells 10 (SOFC-X)*, Eguchi, K., Singhal, S.C., Yokokawa, H. and Mizusaki, J. (eds.). ECS Transactions, 7, 1919-1928.

[11] Yuan, J. and Sundén, B., 2006, Analysis of Chemically Reacting Transport Phenomena in an Anode Duct of Intermediate Temperature SOFCs, *ASME J. Fuel Cell Sci., Tech. and Engn.*, 2, 89-98,.

[12] Aguiar, A., Adjiman, C.S. and Brandon, N.P., 2004, Anode-supported Intermediate Temperature Direct Internal Reforming Solid Fuel Cell. I: Model-based Stead-state Performance. *J. Power Sources,* 138, 120-136.

[13] Mostinsky, I.L., "Diffusion coefficient," in: *International Encyclopedia of Heat & Mass Transfer*, Hewitt, G.F., Shires, G.L. and Polezhaev, Y.V. (eds.), 1996, CRC Press, Florida, USA.

[14] Ferguson, J.R., Fiard, J.M. and Herbin, R., 1996, Three-dimensional Numerical Simulation for Various Geometries of Solid Oxide Fuel Cells. *J. Power Sources,* 58,109-122.

[15] Khaleel, M.A., Rector, D.R., Lin, Z., Johnson, K. and Recknagle, K., 2005, Multiscale Eelctrochemistry Modeling of Solid Oxide Fuel Cells, *Int. J. Multiscale Computational Engineering*, 3, 33-47.

[16] Karakasidis T.E. and Charitidis C.A., 2007, Multiscale Modeling in Nanomaterials Science, *Materials Science and Engineering*, C27, 1082-1089.

Nomenclature

A_{active}	surface area of control volume at active site, m^2
a	width of porous layer, m
B	inertial coefficient
b	width of flow duct, m
c_p	specific heat capacity, J/(kg K)
D	molar diffusion coefficient of fuel gas species, m^2/s
E_a	activation energy, kJ/mol
H	enthalpy, kJ/mol

h	overall height of the duct, m
h_d	height of the duct, m
h_p	thickness of porous layer, m
J	electrochemical reaction related molar flux, mol/(m^2 s)
K_e	equilibrium constants, Pa^2
k	thermal conductivity, W/(m K); reaction rate constant, mol/(m^3 Pa^2 s)
k_0	pre-exponential constant, -
M	molecular weight of species, kg/mol
$\dot{m}$	mass diffusion flux, kg/(m^2 s)
$\dot{n}$	molar diffusion flux, mol/(m^2 s)
n	total number of species, -
P	pressure, Pa
q	heat flux, W/(m^2)
R	internal reforming reaction rate, mol/(m^{3}s)
$\Re$	gas constant, kJ/(mol K)
Re	Reynolds number (UD_h/ν), -
r_e	effective radius, m
S	source term
T	temperature, ^{o}C
$\boldsymbol{v}$	velocity vector, m/s
V_i	velocity components in x, y and z directions, respectively, m/s
X	molar fraction of fuel species, -
Y	mass fraction of fuel species, -
x, y, z	Cartesian coordinates

Greek Symbols

β	permeability of porous layer, m^2
ε	porosity, -
μ	dynamic viscosity, kg/(m s)
ν	kinematic viscosity, m^2/s
ρ	density, kg/m^3
τ	tortuosity, -

Subscripts

di	diffusion layer
eff	effective parameter
f	fuel gas mixture
CH_4	methane
CO	carbon monoxide
CO_2	carbon dioxide
e	equilibrium
gm	fuel gas mixture
H_2	hydrogen
H_2O	water
in	inlet
k	Knudsen diffusion
m	mass transfer
p	permeation
r	steam reforming reaction
s	solid wall; shift reaction; species